Paper IV

Running title:

Morphology and elemental composition of *V. splendidus*

Title:

Changes in morphology and elemental composition of *Vibrio splendidus* along a gradient from carbon-limited to phosphate-limited growth.

Trond Løvdal*, Evy F. Skjoldal, Mikal Heldal, Svein Norland, T. Frede Thingstad

Department of Biology, University of Bergen, Jahnebakken 5,

PO Box 7800, N-5020 Bergen, Norway

*Corresponding author: trond.lovdal@bio.uib.no

Abstract

We examined morphology, elemental composition (C, N, P) and orthophosphate-uptake efficiency in the marine heterotrophic bacterium *Vibrio splendidus* grown in continuous cultures. Eight chemostats were arranged along a gradient of increasing glucose concentrations in the reservoirs, shifting the limiting factor from glucose to phosphate. The content of carbon, nitrogen and phosphorus was measured in individual cells by X-ray microanalysis using a transmission electron microscope (TEM). Cell volumes (V) were estimated from length and width measurements of unfixed, air-dried cells in TEM. There was a transition from coccoid cells in C-limited cultures towards rod-shaped cells in P-limited cultures. Cells in P-limited cultures with free glucose in the media were significantly larger than cells in glucose-depleted cultures ($P < 0.0001$). We found functional allometric relationships between cellular C-, N-, and P-content (in femtograms) and V (in cubic micrometers) in *V. splendidus* ($C = 224 \times V^{0.89}$, $N = 52.5 \times V^{0.80}$, $P = 2 \times V^{0.65}$); i.e., larger bacteria had less elemental C, N, and P per V than smaller cells, and also less P relative to C. Biomass-specific affinity for orthophosphate-uptake in large, P-limited *V. splendidus* approached theoretical maximum values predicted for uptake limited by molecular diffusion towards the cells. Comparing these theoretical values to respective values for the smaller, coccoid, C-limited *V. splendidus* indicated, contrary to the traditional view, that large size did not represent a trade-off when competing for the non-C limiting nutrients.

Introduction

Modern tools of molecular biology have started to give us insight into the species composition and diversity of natural bacterial communities. We need answers to the old question of what physiological mechanisms and what life strategies that control the success of a particular species in a given environment, in order to better understand the internal dynamics between ecologically functional units within the bacterioplankton 'black box' [17]. The need for laboratory experiments to elucidate the theory that relates cell size to mass transfer was pointed out ten years ago by Karp-Boss et al. [9] because the size range examined was very narrow and limited to small-celled bacteria. Small, spherical cells are traditionally believed to be more efficient in their uptake of nutrients because of their large surface-to-volume ratio [cf. 15]. However, based on nutrient diffusion theory, a more precise formulation would be that it is the 'surface : cell requirement of limiting element', rather than the 'surface : volume' ratio, that is important [8, 9, 30]. At low external concentrations, the rate-limiting step for uptake will be the diffusive transport towards the cell. The expression for maximum diffusive transport towards a cell can be expressed as the product of three terms $G \times D \times S$, where G is the conductance of the cell, D is the molecular diffusion constant for the substrate in water, and S the substrate concentration at an infinite distance from the cell. Defining an organism's specific affinity for a substrate as the volume cleared for substrate per unit biomass per unit time, the ability of an osmotroph organism to compete at permanently low substrate concentrations is given by its maximum specific affinity (α_{max}). Assuming that the cell is diffusion-limited, i.e., that the cell's uptake system is so efficient (and the bulk nutrient concentration so low) that all substrate molecules hitting the cell surface are captured, it is possible to derive a theoretical expression for the affinity constant:

$$\alpha_{max} = GD/V\sigma \qquad (1)$$

where V is the volume of the cell, and σ is the volume-specific intracellular content of the element in question [2, 30]. The value of G is determined by the shape of the cell. While it is not possible to give the conductance for all shapes, it is possible to place bounds on the value of G [2]; $G \geq 4\pi r_e$, where r_e is the radius of the equivalent sphere (a sphere with the same volume as the particle being considered). That is, a sphere has the lowest conductance for a given volume. Equation 1 thus illustrates that, for a given volume, non-spherical cells will have a competitive advantage compared to spherical cells with the same internal cell concentration (σ).

From Equation 1 it is possible to derive an expression for a spherical cell of radius r [30]:

$$\alpha_{max} = (4\pi Dr)/m \qquad (2),$$

where m is the amount of the limiting element required to form a new cell. For a conservative substrate not lost by leakage or respiration, m will be the cell quota of the limiting element. Inserting $m = \frac{4}{3}\pi r^3\sigma$ leads to the expression $\alpha_{max} = 3D/\sigma r^2$. For spherical cells with similar σ, α_{max} thus decreases with the inverse square of the cell radius; it may therefore be envisaged that small cells should be superior to larger ones. However, diffusion transport increases in proportion to cell size [8] and heterotrophic bacteria are able to adjust cell quotas according to the availability of substrates [33]. Equation 2 illustrates that if a large size can be obtained with a less than proportional increase in m, large size would actually be an advantage rather than a disadvantage, also at permanently low substrate concentrations.

Thingstad *et al*. [30] suggested that some osmotrophic micro-organisms may obtain a competitive advantage by using a non-limiting element to increase size, without thereby increasing their cellular quota of the limiting element. In an environment where large size also reduces some of the grazing pressure, the otherwise often expected trade-off between competitive and defense ability would disappear, and size increase become a win-win,

"Winnie-the-Pooh" [30] strategy. Note how this may add a new aspect to the advantage of forming cellular storage materials. The traditional explanation for such storage is the potential future fitness of the organism when the storage material can replace the growth-limiting factor in a changed environment. When such accumulation of non-limiting storage material leads to increase in cell size, the mechanism would provide fitness in the actual present situation, in addition to the less certain future prospective. Øvreås *et al.* [36] proposed such a mechanism to explain mesocosm results where a near-natural bacterial community was forced to mineral nutrient-limited growth by adding glucose in excess of bacterial consumption. This did not lead to a shift to small bacteria as one might expect if these were the best competitors for mineral nutrients, but to large-celled *Vibrio splendidus* filled with C-rich granules. The genus *Vibrio* encompasses a diverse and ubiquitous group of bacteria that have long served as models for heterotrophic processes [20, 21, 31], it is, however, uncertain which environmental factors that determines its observed dynamics [31].

The objective of the current study was to characterize how nutritional status is reflected in morphology and elemental composition of *V. splendidus* grown in continuous cultures along a gradient from C- to P-limitation. The combined use of X-ray microanalysis (XRMA) in transmission electron microscopy (TEM) and uptake experiments under a strict set of defined conditions provided data that may contribute to explain the observed variations in bacterial cell size and C:N:P stoichiometry that have been reported [11, 34]. The results suggest that the putative superiority of small, spherical bacteria in nutrient competition should be viewed with some caution.

Materials and Methods

Chemostat set-up

Vibrio splendidus, isolated from the Mediterranean Sea, was kindly provided by dr Philippe Lebaron, Banyuls-sur-Mer. The bacterium was initially grown in batch cultures, first on a rich medium (Difco 0979), before it was transferred to a defined artificial sea water (ASW) medium [35]. The bacterium was passed several times in ASW manipulated to decreasing concentrations of P and N until a final target concentration of 0.64 μmol P L^{-1} and a molar N:P ratio of 44. The same medium supplemented with glucose to final concentrations of 11, 22, 54, 108, 162, 216, 324 and 440 μmol glucose C L^{-1} was fed to eight chemostats numbered 1 through 8, respectively, corresponding to a gradient in supply C:P mole ratio from 17 to 687. Chemostats were of the design described by Pengerud *et al.* [22] using silicon tubing for transporting medium and air into the culture. Medium flow was controlled using an 8-channel Gilson peristaltic pump. Culture volumes were 250 mL and dilution rate 0.02 $hour^{-1}$. Temperature was kept at 20ºC and illumination was continuous. Three weeks after inoculation, an approximate steady state was reached with glucose exhausted from all chemostats. Reservoirs were therefore substituted to give the more extended gradient: 11, 23, 58, 112, 196, 392, 828 and 1706 μmol glucose-C L^{-1}. This gave a gradient in supply C:P molar ratio from 17 to 2666. New approximate equilibria were reached after another three weeks. Only results obtained from the second equilibria are reported. Nutrient limitation of bacteria in Chemostats 1 and 8 were assessed by an organic C (glucose) and a mineral P (KH_2PO_4) enrichment bioassay, respectively. Significant increase in bacterial numbers relative to untreated controls accompanied by consumption of the added substrate after over night incubation verified C-limitation in Chemostat 1 and P-limitation in Chemostat 8 (see below for methods).

Chemical analysis

Glucose was measured spectrophotometrically using the GAGO20 assay kit (Sigma). Samples from the culture media were filtered gently through a sterile Dynagard 0.2-µm pore size syringe filter (Spectrum Laboratories) before analysis. Soluble reactive phosphorus (SRP) was measured according to Koroleff [10]. ASW with no phosphate added was used as a blank in SRP measurements. All spectrophotometry was performed using a Shimadzu UV-1201-V spectrophotometer equipped with a 5-cm kuvette.

Counting of bacteria

Bacteria were counted by flow cytometry (FCM) using a FACSCalibur flow cytometer (Becton Dickinson) equipped with an air-cooled laser providing 15 mW at 488 nm and with standard filter set-up. Bacterial samples were fixed with 25% glutaraldehyde (final concentration, 0.5%) for 30 min at 4ºC, frozen in liquid nitrogen and stored at -70ºC until further analysis. Thawed samples were diluted 10 to 100 fold in TE buffer (Tris 10 mM, EDTA 1 mM, pH 8), stained with SYBR Green-I [14], and analyzed for 1 min at a delivery rate of approximately 40 µL min^{-1} corresponding to an event rate of 100 – 1000 s^{-1}. Known concentrations of fluorescent microspheres (Molecular Probes Inc.) with a diameter of 1 µm were added as an internal standard.

Alkaline phosphatase activity (APA)

APA was measured fluorometrically using 3-*0*-methylfluorescein-phosphate (MFP) as substrate [23]. Samples were mixed with MFP solution in 0.1 mol L^{-1} Trizma-HCl pH 8.3 (final concentration 0.1 µmol L^{-1}). Fluorescence was measured directly after the addition of reagent and at two different time intervals according to the expected activity using the Perkin Elmer fluorometer LS50B. Autoclaved samples were used as blanks.

Uptake of $^{33}PO_4^{3-}$

Uptake of $^{33}PO_4^{3-}$ was measured according to Thingstad *et al*. [29]. Carrier-free $^{33}PO_4^{3-}$ (Amersham Biosciences) was added to 5-mL subsamples in 15-mL sterile Falcon tubes to a final radioactive concentration of approximately 10^6 counts per minute (cpm) mL^{-1}. Samples were incubated at *in situ* temperature and light for an incubation time varying between 20 seconds and 6 hours, according to the expected turnover time. Incubations were stopped by cold chase by addition of cold KH_2PO_4 (1 mmol L^{-1} final concentration). Subsamples were filtered through 0.2-µm pore sized Poretics polycarbonate filters supported on Whatman GF/C filters soaked with 10 mmol L^{-1} KH_2PO_4. Filtrations were done as parallel filtration by use of a Millipore manifold. Portions of 2 mL were filtered on each filter within 30 min after the cold chase. Filters were transferred to scintillation vials with 3 mL Ultima Gold scintillation cocktail (Packard) and radioassayed with a Lumi-One portable scintillation counter (Bioscan Inc.). Fifty µL from the subsamles incubated with $^{33}PO_4^{3-}$ were transferred directly to scintillation vials and mixed with 3 mL scintillation cocktail to measure total added radioactivity in the samples. Trichloroacetic acid-killed samples were used as blanks.

Turnover times (T; h) for PO_4^{3-} were calculated by the equation [29]:

$$T = \frac{t}{-\ln(1-R)}$$

where t is the incubation time and R is the consumed fraction of added $^{33}PO_4^{3-}$. Biomass-specific affinity for orthophosphate uptake (α; L nmol-P^{-1} h^{-1}) was estimated according to the procedure proposed by Thingstad and Rassoulzadegan [28]:

$$\alpha = 1/(TB)$$

where B is the biomass-P (nmol P L^{-1}). In the current experiment, elemental biomass was estimated by multiplication of the mean per-cell content of the element in question (as

obtained in XRMA), and the concentration of bacteria (as obtained in FCM). This method presumably gives better estimates for bacterial biomass than conventional conversion factors.

X-ray microanalysis (XRMA) and cell volume determinations

Total amounts of elements in single cells were measured by transmission electron microscopy (TEM). Bacteria were harvested by centrifugation in a Beckman model L8-70M preparative ultracentrifuge, using a SW41 swing-out rotor for 10 min, at 10,000 rpm (7000 × g) onto 100 mesh aluminium grids (Agar Scientific) with carbon coated formvar film and air dried. Neither fixative nor stain was applied. XRMA was done in a Philips CM 200 TEM equipped with an EDAX light element detector (DX-4) supported by Soft Imaging System (SIS) software. With special designed software the electron beam scan chosen cells/particles and background areas were analyzed at preset conditions (80 kV accelerating voltage, spot size 3 (14 nm)). For calibration of carbon measurements we used latex beads (Agar Scientific), and calibration constants for carbon and other elements were obtained according to Norland *et al.* [18]. Sixteen to 64 bacteria (mean = 46) from each chemostat were analyzed. For a detailed description of calibration procedures, XRMA principals and TEM-XRMA biovolume estimation, see Norland *et al*. [18].

Bacterial size was assessed independently by epifluorescence microscopy. Samples were fixed with 25% glutaraldehyde (final concentration 5%), stained with acridine orange and filtered onto black 0.2 μm pore sized Poretics polycarbonate filters [7]. Stained bacteria were visualized under blue exitation with a Zeiss Axioplan epifluorescence microscope at a magnification of 1000× and photographed with a Nikon D1 digital camera equipped to the microscope. Length (L) and width (W) of stained bacteria was measured from digital photographs opened with the Java based program ImageJ [24] calibrated with fluorescent microspheres (Molecular Probes). Three preparates from each chemostat were photographed,

and size of 20 to 45 bacteria measured in each photograph. Volume of the cells was calculated as $(\pi/4)W^2(L - W/3)$ according to Bratbak [1].

Unless otherwise stated, cell size and volumes obtained by TEM are used.

Calculation of theoretical α_{max}

Theoretical α_{max} for PO_4^{3-} uptake in bacterial cells of spherical and cylindrical shape was calculated according to Equation 1. Expressions for *G* and *V* were taken from Clift *et al*. [2] according to Table 1. *D* was assumed to be $\approx 10^{-5}$ cm^2 s^{-1} for a small molecule like PO_4^{3-}.

Statistical analysis

Statistical analysis was performed according to Sokal and Rohlf [25]. The confidence level for all analyses was set at 95%. The relationship between elemental content of C, N, and P, and cell volume was assessed from logarithmically transformed data in regression analysis by the power-law relationship [19].

Results

Bacterial growth and nutrient consumption

After ten exchanges, most of the transients had died out and changes in cell numbers were less than 30% per day over the last 2 to 3 days. Along the gradient of increasing reservoir glucose concentration, there was an initial linear increase in bacterial density, accompanied by a linear decrease in the concentration of SRP (Figure 1). The slopes of these lines correspond to a constant yield of 1.5×10^{14} cells (mole glucose-C)$^{-1}$ and a constant molar C:P ratio in bacterial consumption of 170. For reservoir C:P ratios above approximately 300, there was a slight decrease in bacterial density. For reservoir C:P ratios between 170 and approximately 530, both orthophosphate and glucose were completely consumed, i.e., indicating almost a

factor of 3 change in the C:P stoichiometry of nutrient consumption in the transition from C- to P-limited growth. For reservoir C:P ratios above approximately 530, additional glucose was not consumed and was found in the cultures as free glucose.

PO_4^{3-} turnover times ranged from > 400 hours in Chemostat 1 to less than one minute in Chemostats 6, 7 and 8, in good agreement with APA ranging from ~1 to > 1500 nmol L^{-1} h^{-1} in the same chemostats, respectively (data not shown). Biomass-specific affinity for PO_4^{3-} was < 0.002 L nmol-P^{-1} h^{-1} in Chemostats 1 to 4, increased to 0.08 L nmol-P^{-1} h^{-1} in Chemostat 5, and 0.207, 0.178 and 0.176 L nmol-P^{-1} h^{-1} in Chemostats 6, 7 and 8, respectively (Figure 2).

Morphology and elemental content

Values for morphometry and cellular content and concentration of C, N, and P at steady state are shown in Table 2. Estimated mean volume of the cells varied from 0.23±0.13 μm^3 in Chemostat 1 to 1.74±0.73 μm^3 in Chemostat 8. The relationship between cellular volume and the 'length to *r* ratio' (*g*) is shown in Figure 3. Along with the increase in cellular volume, there was an increase in *g* from 3.4±1.1 in Chemostat 1 to 7.6±3.1 in Chemostat 8, respectively, illustrating a transition from coccoid to rod-shaped cells along the gradient from C- to P-limited growth. A statistically significant increase in cell volume (*t*-test for sample sizes of unequal number; $P < 0.0001$) was seen in chemostats with free glucose in the cultures. The increase in cell size was accompanied by an increase in the cell quota of both C, N, and P, but with the most pronounced increase in the C-quota (Table 2; Figure 4). The overall geometric mean of the volume-specific elemental C was 251 ± 91 fg C μm^{-3}. Cellular C:N:P ratios were high in all chemostats with values well above the Redfield ratio for algae. Cellular C:P ratios were variable in Chemostat 1 through 6, but were markedly elevated in Chemostats 7 and 8 (Table 2).

Figure 4 shows scatter plots of per cell C, N, and P biomass (Figure 4A, B and C, respectively) versus cell volume. Respective coefficients of correlation for log-transformed values were 0.908, 0.879 and 0.777, and the regression coefficients were 0.825, 0.773 and 0.605, respectively, when pooling the data from all chemostats (n = 371). All the elements investigated had volume scaling factors that were significantly less than unity (t-test for sample sizes of equal number; $P \leq 0.012$), suggesting that the larger *V. splendidus* had less elemental C, N, and P per cell volume than the smaller ones. The volume to P scaling factor was particularly low with an over all value of 0.65 compared to 0.89 and 0.80 for C and N, respectively. Comparison of the slopes of the regression lines (Figure 4) revealed a significant difference between the volume to C and the volume to P scaling factors (F-test; $P < 0.0001$), and also between the volume to N and the volume to P scaling factors (F-test; $P < 0.001$), suggesting that the larger *V. splendidus* had less P relative to C and N than smaller ones.

Bacterial size estimated by TEM and ImageJ showed good correlation (r = 0.979; Figure 5). One exception was found for Chemostat 5 where the mean volume estimated by ImageJ (0.59 ± 0.39 μm^3, n = 114) was 73% larger than that estimated by TEM. Both methods showed large variation in cell size within each of the chemostats, as represented by large standard deviations (SD) in Figure 5. Rejecting Chemostat 5 from statistical analysis did not change the constant terms (Figure 4) but elevated the scale factors by 7 to 14%. However, an omission of the values from Chemostat 5 did not change the confidence limits of any statistical test reported here.

Discussion

Along a gradient from C- to P-limited growth, *V. splendidus* demonstrated a transition from coccoid to rod-shaped cells with a significant increase in cell volume in P-limited cultures with free glucose in the media (Figure 1 and 3). Increase in cell size of P-starved vibrios upon

glucose amendment has been observed before [20, 21], and has been attributed to the intracellular accumulation of the C-rich polymer poly-β-hydroxybutyrate (PHB) [21]. The relative proportional increase in C and N (Figure 4) indicates that C was not stored as PHB in our experiment, but rather that it was incorporated as protein in the cellular machinery. The theoretical benefits calculated from diffusion theory [2, 30], however, will be the same either the non-limiting element is stored as inclusion bodies or assimilated into the cell's functional machinery. *V. splendidus* displayed a great ability to consume organic C by depleting the medium for glucose for a range of reservoir C:P ratios up to approximately 530. Cellular C:N:P ratios were high in all chemostats (Table 2), with values comparable to the reported ratio of 260:37:1 (mol:mol) for *V. splendidus* in glucose-amended mesocosms [36], but well above the 'traditional' ratio of approximately 50:10:1 reported for marine bacteria [4, 5]. Using a pure culture of *Pseudomonas putida* and mixed bacterial populations, Bratbak [1] found that the C:N:P ratio of bacterial biomass changed between 8:2:1 and 500:90:1, depending on the substrate C:N:P ratio. Similar results were observed by Tezuka [27]. In the present experiment, cellular C:N:P ratios increased along the gradient, which could be expected because of an increasing degree of P limitation. However, cellular C:P ratios were unexpectedly high in C-limited cultures; in Chemostat 1 the cellular C:P ratio was approximately ten times that of the C:P ratio of the reservoir. If one compares the C-limited Chemostat 1 to the P-limited Chemostat 8, a > 150 fold increase in reservoir C:P ratio led only to a two fold increase in cellular C:P ratio. Thus, it does not seem that the C:P ratio of *V. splendidus* biomass is determined by the substrate C:P ratio to the same degree as reported for other bacteria [1, 27]. The volume-specific scaling factor for C found in this study (Figure 4A) is comparable to the factors reported for volume-specific dry weight [13, 19], and volume-specific elemental cell content of C, N, and P [6]. The volume to C scaling factor was, however, significantly higher than the volume to P scaling factor (Figure 4C). This

implies that *V. splendidus* increased its volume by increasing the intracellular content of C without a proportional increase in intracellular P.

Figure 2 show that the estimated biomass-specific affinity in the large, P-limited cells of Chemostat 6 – 8 approached the theoretical maximum assuming diffusion transport towards the cells to be the rate-limiting step. The theoretical maximum values of the larger *V. splendidus* are lower than those for the small cells in the C-limited cultures (Figure 2), however, not to an extent that would represent a trade-off in nutrient competition. In a recent review of published data, Flaten *et al.* (unpubl.) reported an array of bacterial biomass-specific affinity values, both from laboratory and field studies. Compared with these values (Flaten et al. unpubl.), our estimates for P-limited *V. splendidus* are high. Of 14 listed values for bacterial biomass-specific affinity (Flaten et al. unpubl.), only environmental samples from the ultraoligotrophic eastern Mediterranean Sea, which reached maximum values up to 0.22 L nmol-P^{-1} h^{-1} for the size fraction between 0.2 – 0.6 μm [16], and a chemostat grown (dilution rate 0.012 h^{-1}) P-limited [*Pseudomonas*] *paucimobilis* (now transferred to the genus *Sphingomonas* [26]) isolated from Lake Memphremagog, which reached maximum values up to 0.15 L nmol-P^{-1} h^{-1} [3], are comparable to our values. Interestingly, the latter was grown with excess glucose and showed great plasticity in size and were much larger when grown under P-limitation than under C-limitation [3], however, no data on the C:P stoichiometry was reported. Bratbak [1] showed that P-limited *Pseudomonas putida* had a C:P ratio of 500 and a P-biomass corresponding to ~ 0.1 fmol μm^{-3} in the late logarithmic phase of growth, compared to 56 and ~ 0.8 fmol μm^{-3}, respectively, for a mixed bacterial community grown at the same conditions. Taken together, this may indicate that these species (*V. splendidus*, *P. putida*, and *S. paucimobilis*) within the family of *Proteobacteria* all belong to the proposed class of "Winnie-the-Pooh" bacteria. Using the traditional C:P (mol:mol) conversion factor of 50 for bacterial biomass [4, 5] and the widely cited constant factor of 20 fg C per cell for cells

in the size range 0.036 to 0.073 μm^3 [12], small bacterial cells can be estimated to have a P biomass in the range 0.2 – 0.4 fmol μm^{-3}, which are high compared to what we found for *V. splendidus* (Table 2). Using a method similar to us, Fagerbakke *et al.* [4] found that native aquatic bacteria in the size range from 0.11 to 0.41 μm^3 had a P-biomass corresponding to 0.07 – 0.15 fmol μm^{-3}. Our data for the P-limited *V. splendidus* is in the lower end of this range (Table 2).

The effect of reducing the internal concentration of the limiting nutrient on biomass-specific affinity is illustrated in Figure 6A. The plot points out the two hypothesized strategies for heterotrophic bacteria, either to maximize uptake by being small (high surface to volume ratio), or by being large keeping the internal cell quota of limiting element (m) low (high surface to limiting element ratio). As an example, a 2-μm^3 spherical cell with an internal concentration of 0.04 fmol P μm^{-3} will in theory have the same ability to compete for P as 1-μm^3 and 0.5-μm^3 spherical cells with 0.06 and 0.1 fmol P μm^{-3}, respectively. According to theory [2], the transition from coccoid to rod-shaped cells (Figure 3) may give a small additional advantage, in terms of enhanced uptake efficiency. The effect of particle shape upon α_{max} can be theoretically determined from Equation 1 and is illustrated in Figure 6B showing how, for any given volume, cylindrical shape represents a competitive advantage compared to spherical shape. As an example, 0.7-μm^3 rod-shaped (g = 10) and 0.6-μm^3 rod-shaped (g = 5) cells with internal concentrations of 0.1 fmol P μm^{-3} will in theory have the same ability to compete for P as a 0.5-μm^3 spherical cell with the same internal concentration of P. That is, *V. splendidus* may benefit not only from a change in size and elemental composition, but also from a change in shape.

Although the results of this study cannot be applied directly to the natural environment, the results obtained are consistent with observations from mesocosms [36] that demonstrated the success of *V. splendidus* under mineral nutrient-limiting – excess glucose

conditions [cf. 30, this study]. We thus hypothesize that *V. splendidus* represents an active subgroup within the bacterial community with the ability to use a non-limiting resource (glucose) to change its stoichiometry and morphology in a manner increasing its nutrient uptake efficiencies. As opposed to the traditional view that the C-storage provides potential fitness for future C-limited conditions, the size, shape and stoichiometry of *V. splendidus* is thus suggested to provide also instant fitness in situations with mineral nutrient competition. Whether the increase in size and change in shape also serves to reduce predation pressure, and whether *V. splendidus* thus should be classified as belonging to the suggested class of "Winnie-the-Pooh" specialists was not investigated in this study. Our findings corroborate that the putative superiority of small heterotrophic bacteria in nutrient uptake should be viewed with some caution [30, 32], and the recent observations [6, 11, 34, 36] that demonstrate the need of using accurate and locally derived cell volume estimates and elemental conversion factors in biomass assessment of bacteria.

Acknowledgements

This work was supported by the Strategic Institution Programme “Patterns in Biodiversity” Contract 158936/S40 from the Research Council of Norway. The FACSCalibur flow cytometer was in part funded by a grant from The Knut and Alice Wallenberg Foundation to the Virtue program. We gratefully thank Philippe Lebaron for providing the *V. splendidus* culture, Tsuneo Tanaka for advice and assistance, George Jackson for providing information on diffusion literature, and Egil S. Erichsen for his assistance at the Laboratory for Electron Microscopy (LEM), Science Faculty, University of Bergen.

References

1. Bratbak, G (1985) Bacterial biovolume and biomass estimations. Appl Environ Microbiol 49: 1488-1493
2. Clift, R, Grace, JR, Weber, ME (1978) Bubbles, drops, and particles. Academic Press. New York
3. Currie, DJ, Kalff, J (1984) A comparison of the abilities of freshwater algae and bacteria to acquire and retain phosphorus. Limnol Oceanogr 29: 298-310
4. Fagerbakke, KM, Heldal, M, Norland, S (1996) Content of carbon, nitrogen, oxygen, sulfur and phosphorus in native aquatic and cultured bacteria. Aquat Microb Ecol 10: 15-27
5. Goldman, JC, Caron, DA, Dennet, MR (1987) Regulation of gross growth efficiency and ammonium regeneration in bacteria by substrate C:N ratio. Limnol Oceanogr 32: 1239-1252
6. Gundersen, K, Heldal, M, Norland, S, Purdie, DA, Knap, AH (2002) Elemental C, N, and P cell content of individual bacteria collected at the Bermuda Atlantic time-series study (BATS) site. Limnol Oceanogr 47: 1525-1530
7. Hobbie, JE, Daley, RJ, Jasper, S (1977) Use of nuclepore filters for counting bacteria by fluorescence microscopy. Appl Environ Microbiol 33: 1225-1228
8. Jumars, PA, Deming, JW, Hill, PS, Karp-Boss, L, Yager, PL, Dade, WB (1993) Physical constraints on marine osmotrophy in an optimal foraging context. Mar Microb Food Webs 7: 121-159
9. Karp-Boss, L, Boss, E, Jumars, PA (1996) Nutrient fluxes to planktonic osmotrophs in the presence of fluid motion. Oceanogr Mar Biol Ann Rev 34: 71-107
10. Koroleff, F (1983) Determination of phosphorus. In: Grasshoff, K, Erhardt, M and Kremling, K (Ed.) Methods in seawater analysis. Verlag Chemie. pp 125-131
11. La Ferla, R, Leonardi, M (2005) Ecological implications of biomass and morphotype variations of bacterioplankton: an example in a coastal zone of the Northern Adriatic Sea (Mediterranean). Mar Ecol 26: 82-88
12. Lee, S, Fuhrman, JA (1987) Relationships between biovolume and biomass of naturally derived marine bacterioplankton. Appl Environ Microbiol 53: 1298-1303
13. Loferer-Krößbacher, M, Klima, J, Psenner, R (1998) Determination of bacterial cell dry mass by transmission electron microscopy and densitometric image analysis. Appl Environ Microbiol 64: 688-694
14. Marie, D, Partensky, F, Jacquet, S, Vaulot, D (1997) Enumeration and cell cycle analysis of natural populations of marine picoplankton by flow cytometry using the nucleic acid stain SYBR Green I. Appl Environ Microbiol 63: 186-193
15. Morita, RY (1982) Starvation-survival of heterotrophs in the marine environment. Adv Microb Ecol 6: 171-198
16. Moutin, T, Thingstad, TF, van Wambeke, F, Marie, D, Slawyk, G, Raimbault, P, Claustre, H (2002) Does competition for nanomolar phosphate supply explain the predominance of the cyanobacterium *Synechococcus*? Limnol Oceanogr 47: 1562-1567
17. Nishimura, Y, Kim, C, Nagata, T (2005) Vertical and seasonal variations of bacterioplankton subgroups with different nucleic acid contents: Possible regulation by phosphorus. Appl Environ Microbiol 71: 5828-5836
18. Norland, S, Fagerbakke, KM, Heldal, M (1995) Light element analysis of individual bacteria by X-ray microanalysis. Appl Environ Microbiol 61: 1357-1362
19. Norland, S, Heldal, M, Tumyr, O (1987) On the relation between dry matter and volume of bacteria. Microb Ecol 13: 95-101
20. Novitsky, JA, Morita, RY (1976) Morphological characterization of small cells resulting from nutrient starvation of a psychrophilic marine vibrio. Appl Environ Microbiol 32: 617-622
21. Nyström, T, Olsson, RM, Kjelleberg, S (1992) Survival, stress resistance, and alterations in protein expression in the marine *Vibrio* sp. strain S14 during starvation for different individual nutrients. Appl Environ Microbiol 58: 55-65
22. Pengerud, B, Skjoldal, EF, Thingstad, TF (1987) The reciprocal interactions between degradation of glucose and ecosystem structure. Studies in mixed chemostat cultures of marine bacteria, algae, and bacterivorous nanoflagellates. Mar Ecol Prog Ser 35: 111-117
23. Perry, MJ (1972) Alkaline phosphatase activity in subtropical Central North Pacific waters using a sensitive fluorometric method. Mar Biol 15: 113-119
24. Rasband, W (2004) ImageJ. [Online] http://rsb.info.nih.gov/ij/.
25. Sokal, RR, Rohlf, FJ (1995) Biometry, 3rd ed. W.H. Freeman.
26. Takeuchi, M, Sawada, H, Oyaizu, H, Yokota, A (1994) Phylogenetic evidence for *Sphingomonas* and *Rhizomonas* as nonphotosynthetic members of the alpha-4 subclass of the *Proteobacteria*. Int J Syst Bacteriol 44: 308-314

27. Tezuka, Y (1990) Bacterial regeneration of ammonium and phosphate as affected by the carbon:nitrogen:phosphorus ratio of organic substrates. Microb Ecol 19: 227-238
28. Thingstad, TF, Rassoulzadegan, F (1999) Conceptual models for the biogeochemical role of the photic zone microbial food web, with particular reference to the Mediterranean Sea. Prog Oceanogr 44: 271-286
29. Thingstad, TF, Skjoldal, EF, Bohne, RA (1993) Phosphorus cycling and algal-bacterial competition in Sandsfjord, western Norway. Mar Ecol Prog Ser 99: 239-259
30. Thingstad, TF, Øvreås, L, Egge, JK, Løvdal, T, Heldal, M (2005) Use of non-limiting substrates to increase size; a generic strategy to simultaneously optimize uptake and minimize predation in pelagic osmotrophs? Ecol Lett 8: 675-682
31. Thompson, JR, Randa, MA, Marcelino, LA, Tomita-Mitchell, A, Lim, E, Polz, MF (2004) Diversity and dynamics of a North Atlantic coastal *Vibrio* community. Appl Environ Microbiol 70: 4103-4110
32. Vadstein, O (1998) Evaluation of competitive ability of two heterotrophic planktonic bacteria under phosphorus limitation. Aquat Microb Ecol 14: 119-127
33. Vadstein, O, Jensen, A, Olsen, Y, Reinertsen, H (1988) Growth and phosphorus status of limnetic phytoplankton and bacteria. Limnol Oceanogr 33: 489-503
34. Vrede, K, Heldal, M, Norland, S, Bratbak, G (2002) Elemental composition (C, N, P) and cell volume of exponentially growing and nutrient-limited bacterioplankton. Appl Environ Microbiol 68: 2965-2971
35. Wyman, M, Gregory, RPF, Carr, NG (1985) Novel role of phycoerythrin in a marine cyanobacterium, *Synechococcus* strain Dc2. Science 230: 818-820
36. Øvreås, L, Bourne, D, Sandaa, R-A, Casamayor, EO, Benlloch, S, Goddard, V, Smerdon, G, Heldal, M, Thingstad, TF (2003) Response of bacterial and viral communities to nutrient manipulations in seawater mesocosms. Aquat Microb Ecol 31: 109-121

Table 1

Expressions for conductance (G) and volume (V) for spheres and cylinders. Taken from Clift *et al*. [2]. r = radius, g = length/r.

Object shape	G	V
Sphere	$4\pi r$	$\frac{4}{3}\pi r^3$
Cylinder thin rod; $g > 20$	$\frac{2\pi r g}{\ln g}$	$\pi r^3 g$
Cylinder short rod; $0 < g \leq 16$	$(8 + 4.10 g^{0.76})r$	$\pi r^3 g$

Table 2

Morphometric values and C, N, P content and concentration of bacteria from the chemostats. Means of single-cell measurements with standard deviations. Molar C:N:P ratios are derived from means of single-cell concentration measurements. *n*: number of cells analyzed.

Chemostat no.	Length (µm)	Width (µm)	Volume (μm^3)	Element content (fg $cell^{-1}$)			Element concentration (fmol μm^{-3})			C:N:P ratio (mol:mol)	*n*
				C	N	P	C	N	P		
1	0.97 ± 0.23	0.6 ± 0.16	0.23 ± 0.13	55 ± 26	12 ± 6	0.8 ± 0.3	21.4 ± 8.5	3.9 ± 1.5	0.13 ± 0.07	165:30:1	36
2	1.56 ± 0.5	0.71 ± 0.15	0.54 ± 0.29	101 ± 51	23 ± 12	0.9 ± 0.5	17.1 ± 5.3	3.4 ± 1.1	0.06 ± 0.02	285:57:1	42
3	1.72 ± 0.47	0.72 ± 0.19	0.59 ± 0.25	118 ± 36	32 ± 8	1.4 ± 0.4	18.0 ± 4.9	4.3 ± 1.4	0.09 ± 0.03	200:48:1	58
4	1.15 ± 0.3	0.71 ± 0.23	0.37 ± 0.22	65 ± 28	21 ± 9	0.7 ± 0.5	17.5 ± 7.7	4.9 ± 2.3	0.08 ± 0.06	219:61:1	16
5	1.42 ± 0.45	0.59 ± 0.16	0.34 ± 0.2	96 ± 29	29 ± 8	1.4 ± 0.4	27.2 ± 8.1	7.2 ± 2.2	0.15 ± 0.05	181:48:1	53
6	2.49 ± 0.74	0.77 ± 0.13	1.05 ± 0.49	209 ± 72	53 ± 16	2.3 ± 0.8	17.7 ± 4.6	3.9 ± 1.0	0.08 ± 0.02	221:49:1	64
7	2.96 ± 1.1	0.88 ± 0.2	1.61 ± 0.8	532 ± 242	103 ± 50	3.3 ± 1.6	28.8 ± 6.7	4.8 ± 1.4	0.07 ± 0.02	411:69:1	45
8	3.18 ± 0.97	0.88 ± 0.17	1.74 ± 0.73	371 ± 124	83 ± 25	3.1 ± 1.3	19.0 ± 5.4	3.7 ± 1.1	0.06 ± 0.03	317:62:1	57

Figure 1

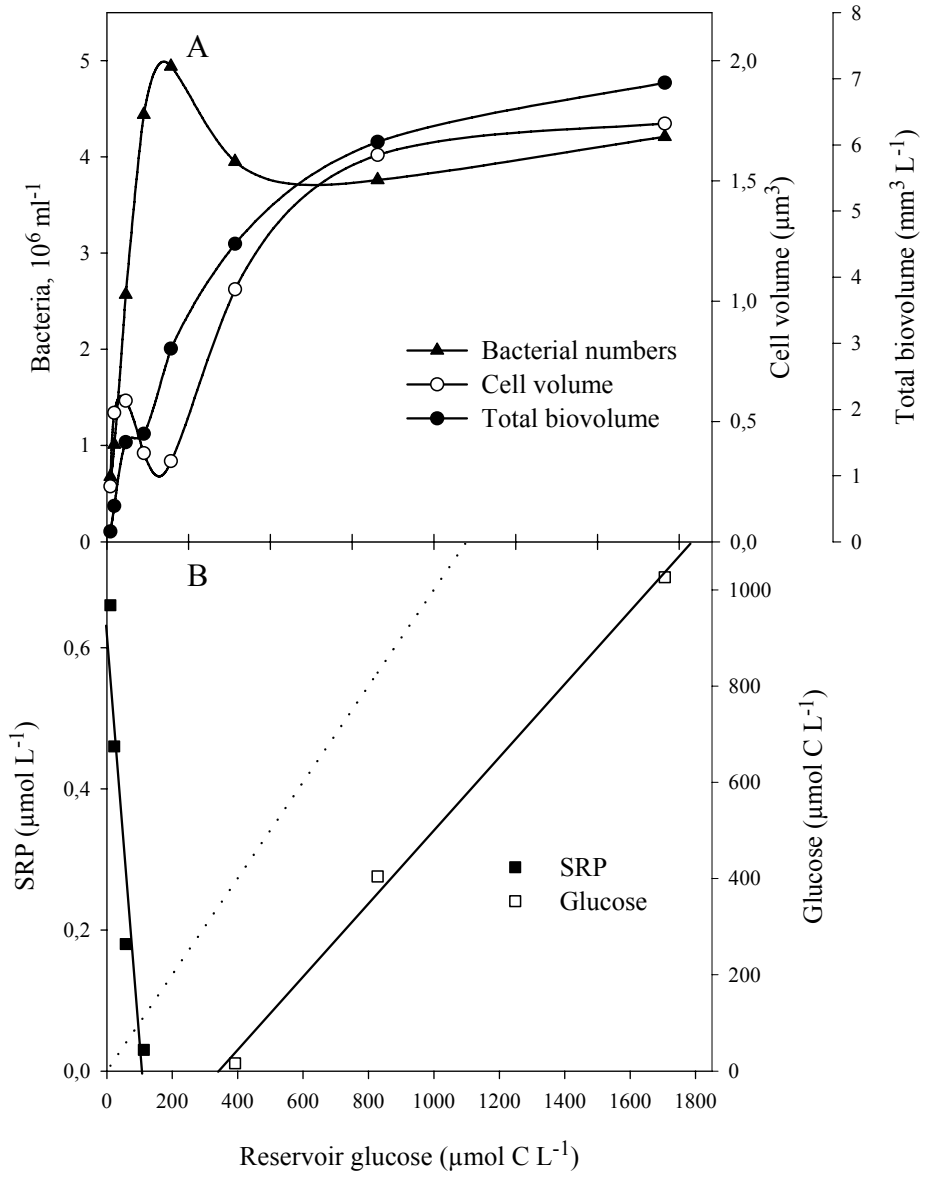

Figure 1. Effect of reservoir glucose concentration on (A) bacterial numbers, cell volume and total biovolume, and (B) culture concentrations of SRP and glucose. SRP and glucose data are shown with regression lines between detectable concentrations. Dotted line: culture glucose concentration in the hypothetical case of no degradation.

Figure 2

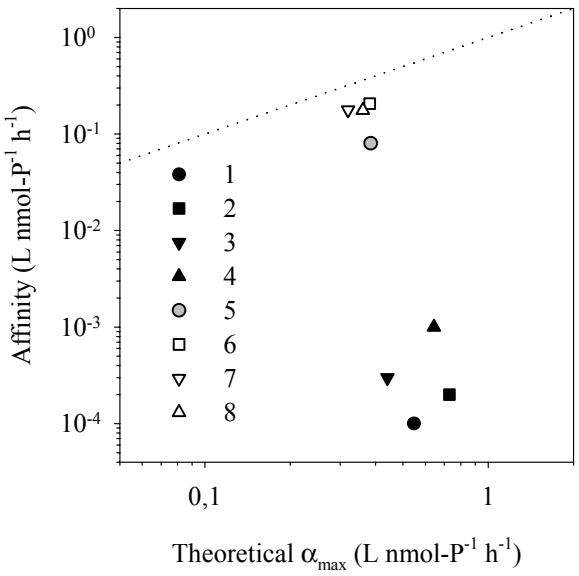

Figure 2. Estimated mean biomass-specific affinity for PO_4^{3-} uptake versus the theoretical maximum values in Chemostat 1 through 8. Black symbols denote cultures with detectable SRP concentrations but undetectable glucose concentrations in the media. White symbols denote cultures with undetectable SRP concentrations but detectable glucose concentrations in the media. Neither SRP nor glucose was detectable in the medium of Chemostat 5 (grey symbol). Dotted line denotes a 1:1 relationship.

Figure 3

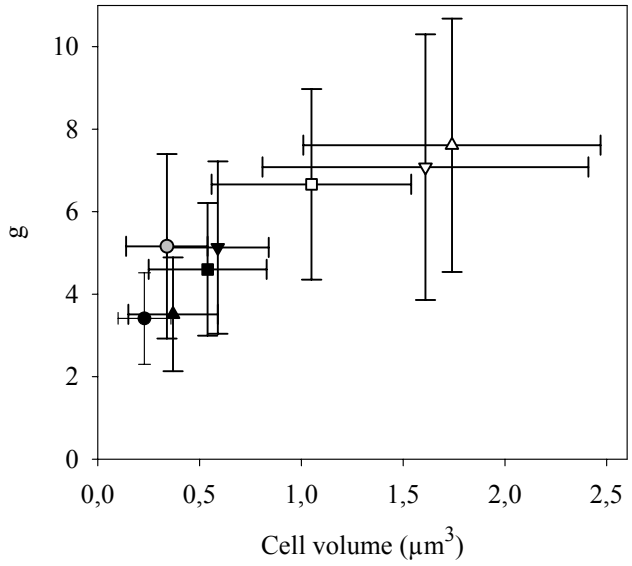

Figure 3. *g* versus cell volume in Chemostat 1 through 8 (legends as in Figure 2). Means of single-cell measurements with standard deviations.

Figure 4

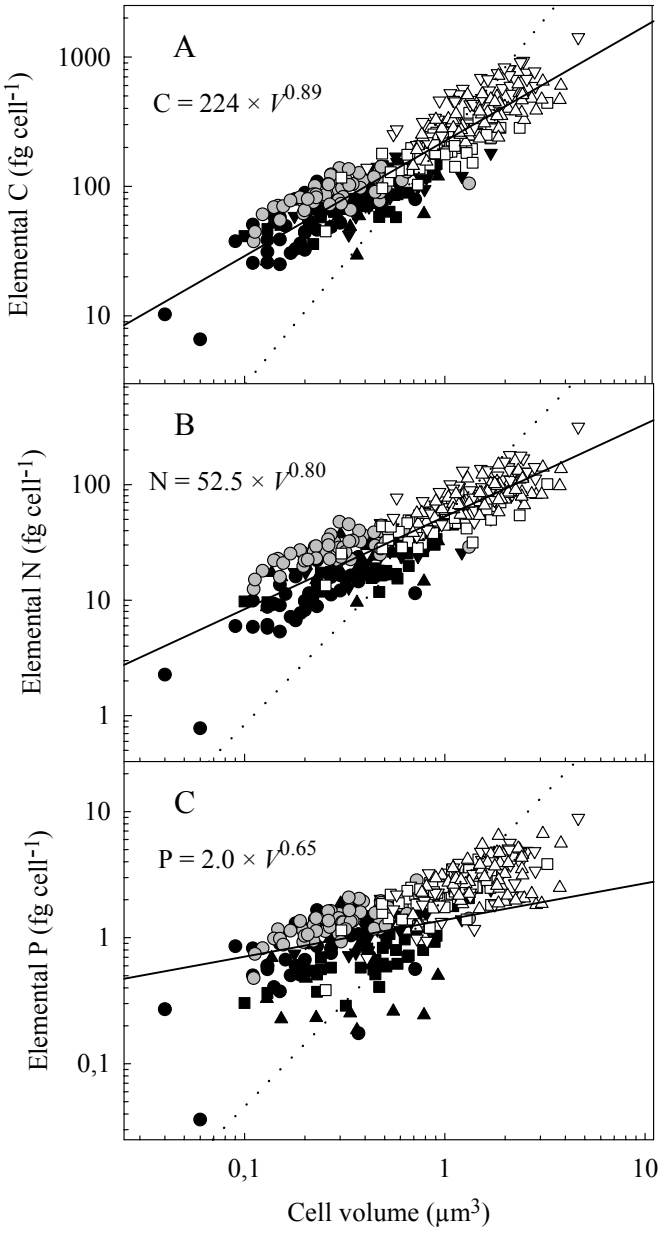

Figure 4. Log-log plot of the relationship between cell volume and cellular content of (A) C, (B) N, and (C) P in single bacteria of Chemostat 1 through 8 (legends as in Figure 2). The dotted lines were plotted using a scaling factor of one.

Figure 5

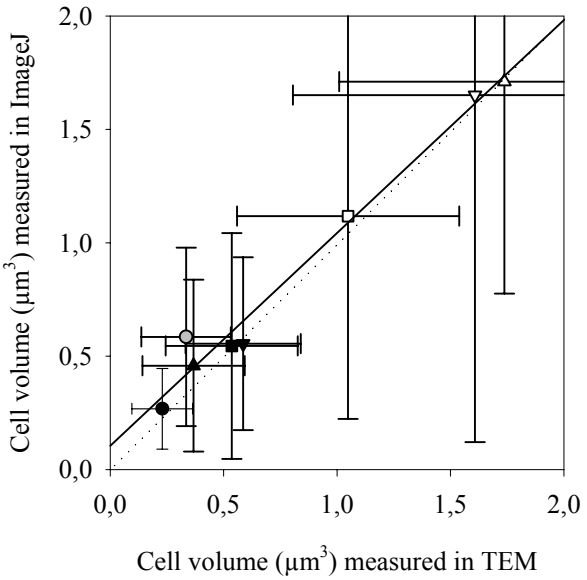

Figure 5. Comparison of cell volumes measured in TEM and ImageJ. Means of single-cell measurements with standard deviations (legends as in Figure 2). Dotted line denotes a 1:1 relationship.

Figure 6

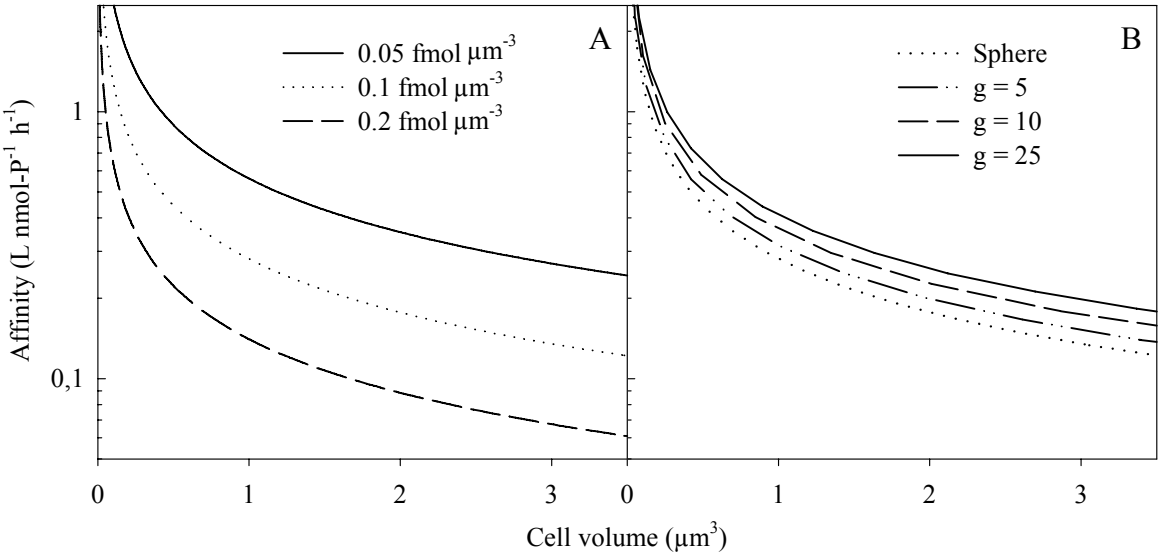

Figure 6. (A) Theoretical α_{max} for PO_4^{3-} uptake versus cell volume for spherical cells with different internal concentrations of P, and (B) for spherical and rod-shaped cells of different *g* assuming an internal P concentration of 0.1 fmol µm^{-3} estimated according to Equation 1 with values for *G* and *V* according to Table 1. Thus, the dotted lines in panel A and B are identical, but are presented for illustrative reasons.